Monthly Notices of the ROYAL ASTRONOMICAL SOCIETY

MNRAS **470**, 2262–2269 (2017) doi:10.1093/mnras/stx1391
Advance Access publication 2017 June 7

The segregation of baryons and dark matter during halo assembly

Shihong Liao,[1★] Liang Gao,[1,2] Carlos S. Frenk,[2] Qi Guo[1] and Jie Wang[1]

[1] *Key Laboratory for Computational Astrophysics, National Astronomical Observatories, Chinese Academy of Sciences, Beijing 100012, China*
[2] *Institute of Computational Cosmology, Department of Physics, University of Durham, Science Laboratories, South Road, Durham DH1 3LE, UK*

Accepted 2017 June 3. Received 2017 March 16; in original form 2016 October 24

ABSTRACT

The standard galaxy formation theory assumes that baryons and dark matter are initially well mixed before becoming segregated due to radiative cooling. We use non-radiative hydrodynamical simulations to explicitly examine this assumption and find that baryons and dark matter can also be segregated due to different characteristics of gas and dark matter during the buildup of the halo. As a result, baryons in many haloes do not originate from the same Lagrangian region as the dark matter. When using the fraction of corresponding dark matter and gas particles in the initial conditions (the 'paired fraction') as a proxy of the dark matter and gas segregation strength of a halo, on average about 25 per cent of the baryonic and dark matter of the final halo are segregated in the initial conditions. This is at odds with the assumption of the standard galaxy formation model. A consequence of this effect is that the baryons and dark matter of the same halo initially experience different tidal torques and thus their angular momentum vectors are often misaligned. The degree of the misalignment is largely preserved during later halo assembly and can be understood with the tidal torque theory. The result challenges the precision of some semi-analytical approaches that utilize dark matter halo merger trees to infer properties of gas associated with dark matter haloes.

Key words: methods: numerical – galaxies: haloes – galaxies: structure.

1 INTRODUCTION

The standard galaxy formation theory is based on a two-stage paradigm put forward by White & Rees (1978) and White & Frenk (1991): (i) the dominant mass component, cold dark matter (CDM), collapses by gravitational instability and forms dark matter haloes hierarchically in the ΛCDM cosmological model (see Frenk & White 2012, and references therein); (ii) baryonic matter (gas) condenses in dark matter potential wells due to a series of dissipative and non-linear baryonic processes (e.g. shock-heating, radiative cooling, etc.), and forms luminous galaxies; see the reviews of Benson (2010) and Somerville & Davé (2015).

In this scenario of galaxy formation, a critical assumption is that baryons follow dark matter tightly before experiencing radiative cooling. More specifically, it is assumed that the gas and dark matter, which later form a virialized halo, are initially well mixed and hence distributed in the same Lagrangian region. Under this assumption, the merger trees of dark matter haloes constructed from pure dark matter simulations are often used as the skeleton to calculate baryonic evolution in semi-analytical models (SAs; see e.g. Kauffmann et al. 1999; Springel et al. 2001; Guo et al. 2011). By incorporating baryonic processes with dark matter halo merger trees, SAs achieve great successes in explaining a large body of observational data. We refer the reader to Baugh (2006), Benson (2010), Somerville & Davé (2015) and Knebe et al. (2015) for general reviews and lists of references of SAs.

This assumption is fundamental to galaxy formation theory and is not often questioned. However, given that the underlying physics of gas and dark matter is not entirely the same, i.e. the former is collisional and reaches equilibrium through shocks, while the latter is collisionless and becomes virialized via violent relaxation (Lynden-Bell 1967); the validation of this assumption is not obvious for hierarchically assembled CDM haloes. Indeed, recently some studies have questioned this assumption. For example, Benítez-Llambay et al. (2013) show that the gas in a low-mass halo can be efficiently removed by ram pressure when it crosses a large-scale pancake. This 'cosmic web stripping' mechanism illustrates that the dark matter and gas content of a halo could be initially segregated in the absence of radiative cooling. Another example is that using non-radiative *N*-body/SPH simulations, van den Bosch et al. (2002) found a significant misalignment between the angular momentum vectors of gas and dark matter in haloes, with a median misalignment angle $\theta \approx 27\overset{\circ}{.}1$ and with large scatter. This result is also at odds with the well-mixing assumption discussed above and questions the popular disc formation model (see e.g. Fall & Efstathiou 1980; Mo, Mao & White 1998). The results of van den Bosch et al. (2002) have been confirmed by other hydrodynamical simulations (e.g. Chen, Jing & Yoshikaw 2003; van den Bosch, Abel & Hernquist 2003; Yoshida et al. 2003; Sharma & Steinmetz

★ E-mail: shliao@nao.cas.cn

2005; Croft et al. 2009; Bett et al. 2010; Hahn, Teyssier & Carollo 2010; Zjupa & Springel 2017).

In the disc formation model, the gas, which ultimately ends up in a galactic disc due to radiative cooling, is assumed to share the same initial specific angular momentum as its dark matter halo because of the following reasons: (i) in the classical tidal torque theory (Hoyle 1951; Peebles 1969; Doroshkevich 1970; White 1984; Catelan & Theuns 1996), a halo acquires its angular momentum by tidal torques from the surrounding inhomogeneities (ii) in the linear regime, the gas and dark matter of a halo are initially well mixed and thus experience the same tidal torques and have identical angular momentum vectors (Fall & Efstathiou 1980).

While the angular momentum misalignment has been widely known, its origin is still not yet fully understood (Sharma, Steinmetz & Bland-Hawthorn 2012; Prieto et al. 2015). In this paper, we perform non-radiative hydrodynamical simulations to examine explicitly the fundamental assumption of the mixing in the standard galaxy formation theory. If it does not hold, i.e. the dark matter and gas of a halo are initially segregated, then the tidal torques they experience and thus their angular momentum vectors may not necessarily be identical; this provides a natural solution to the angular momentum misalignment puzzle.

The paper is organized as follows. In Section 2, we present our numerical simulations. We investigate the gas–dark matter segregation of halo in Section 3 and its causes in Section 4. As an application, we use it to explain the angular momentum misalignment between gas and dark matter of haloes in Section 5. Section 6 summarizes and discusses our results. We present numerical convergence studies in the appendix.

2 NUMERICAL SIMULATIONS

We use a Tree-PM *N*-body/SPH code, GADGET-2 (Springel 2005), to perform a set of non-radiative hydrodynamical simulations. The fiducial simulation is a run with 256^3 dark matter and 256^3 gas particles ($256^3 \times 2$) in a periodic box with a comoving length $L_{\rm box} = 10\ h^{-1}$ Mpc on one side. The reason we choose such a small volume is that the box size has negligible effect on the problem studied in this paper (see e.g. Chen et al. 2003; Sharma & Steinmetz 2005; Croft et al. 2009; Bett et al. 2010; Hahn et al. 2010; Zjupa & Springel 2017). The cosmological parameters adopted in the simulations are $\Omega_m = 0.30$, $\Omega_b = 0.04$, $\Omega_\Lambda = 0.70$, $\sigma_8 = 0.9$ and $n_s = 0.96$. Thus, the mass of the dark matter and gas particles are $m_{\rm dm} = 4.3 \times 10^6\ h^{-1}\,{\rm M}_\odot$ and $m_{\rm gas} = 6.6 \times 10^5\ h^{-1}\,{\rm M}_\odot$, respectively. The softening lengths for both dark matter and gas particles are $\epsilon = 1\ h^{-1}$ kpc in comoving units, i.e. about 1/40 of the interparticle separation.

We use the N-GenIC code[1] to generate the initial condition at redshift $z_{\rm ini} = 127$ assuming the total matter distribution follows the linear power spectrum given by Eisenstein & Hu (1998). In the initial conditions, it is assumed that the gas follows the dark matter perfectly in phase space. To achieve this, the N-GenIC code adopts the following set-up. First, $N_p = 256^3$ 'original' particles are used to sample the total matter (including both dark matter and gas) density distribution by perturbing the positions and velocities of a glass particle distribution (White 1996) with the Zel'dovich approximation (Zel'dovich 1970). Then each 'original' particle is split into a dark matter and a gas particle by displacing their positions as

$$\boldsymbol{r}_{\rm dm} = \boldsymbol{r}_{\rm ori} + \frac{1}{2}\frac{\Omega_b}{\Omega_m}\bar{L}\hat{\boldsymbol{r}},$$
$$\boldsymbol{r}_{\rm gas} = \boldsymbol{r}_{\rm ori} - \frac{1}{2}\frac{\Omega_m - \Omega_b}{\Omega_m}\bar{L}\hat{\boldsymbol{r}}, \tag{1}$$

where $\boldsymbol{r}_{\rm ori}$, $\boldsymbol{r}_{\rm dm}$ and $\boldsymbol{r}_{\rm gas}$ are the position of the 'original', dark matter and gas particle, respectively, $\bar{L}$ is the mean interparticle separation of the 'original' particle set, i.e. $\bar{L} = L_{\rm box}/N_p^{1/3}$, and $\hat{r} = (1, 1, 1)$. The velocities of the resulting dark matter and gas particles are set to be identical to the velocity of their 'original' particle, i.e.

$$\boldsymbol{v}_{\rm dm} = \boldsymbol{v}_{\rm gas} = \boldsymbol{v}_{\rm ori}. \tag{2}$$

The masses of a dark matter and a gas particle are

$$m_{\rm dm} = \frac{\Omega_m - \Omega_b}{\Omega_m} m_{\rm ori} \tag{3}$$

and

$$m_{\rm gas} = \frac{\Omega_b}{\Omega_m} m_{\rm ori}, \tag{4}$$

respectively. By doing so, a perfectly mixed distribution for both dark matter and gas are obtained.

To carry out numerical convergence tests, we perform two additional simulations with $128^3 \times 2$ and $512^3 \times 2$ particles, respectively, starting from the initial conditions generated with the same random phases as that of our fiducial $256^3 \times 2$ run. These two simulations are evolved to $z = 2$. The resolution convergence studies are presented in the appendix. In addition, we run another $256^3 \times 2$ simulation with the same simulation set-up but starting from a grid initial condition. We confirm that adopting grid or glass initial conditions does not affect our conclusions. In the main text, we only present the results from our fiducial simulation with a glass set-up.

We adopt the AMIGA HALO FINDER (AHF; Knollmann & Knebe 2009) to identify dark matter haloes from our simulations with a virial overdensity parameter of $\Delta_{\rm vir} = 200$ measured with respect to the mean density. Only haloes with $\geq$2000 dark matter particles and $\geq$2000 gas particles are considered in this study (see the appendix). In total, there are 227 haloes in our sample, for which the lowest mass is $M_{200} \approx 1.0 \times 10^{10}\ h^{-1}\,{\rm M}_\odot$.

3 GAS AND DARK MATTER SEGREGATION

In order to have a direct impression of whether the gas and the dark matter components of a present day halo are initially segregated, at $z = 0$ we select four random haloes. These haloes have masses of $\sim 2 \times 10^{11}\,h^{-1}\,{\rm M}_\odot$. We then trace all the particles inside the virial radius, R_{200}, of each halo back to the initial conditions. We show a projection of their positions in Fig. 1. Such a trace-back particle configuration is dubbed a 'protohalo' in the rest of the paper. If the dark matter and gas of a halo are initially well mixed, the regions occupied by both components should overlap. Quite surprisingly, as seen in the figure, the dark matter (black dots) and the gas (red dots) of all selected haloes are segregated in the initial conditions, although to different degrees. For the first halo (panel a), most of the dark matter and gas particles indeed occupy the same Lagrangian region, but it is easy to see a lack of gas counterparts on the top and bottom corners. The second case (panel b) is quite puzzling. A disjoint clump of dark matter, a few Mpc away from the dominant clump, appears in the final halo, whilst the gas particle counterparts are completely missing. The last two protohaloes (panels c and d)

[1] http://wwwmpa.mpa-garching.mpg.de/gadget

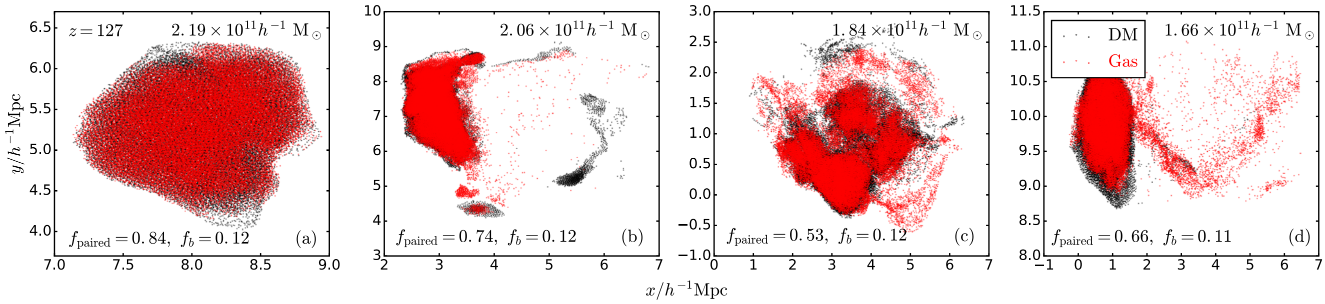

Figure 1. Particle distribution of four randomly selected protohaloes in the initial conditions ($z = 127$). Dark matter and gas particles are shown as black and red dots, respectively. All particles are projected on to the $x - y$ plane in comoving coordinates.

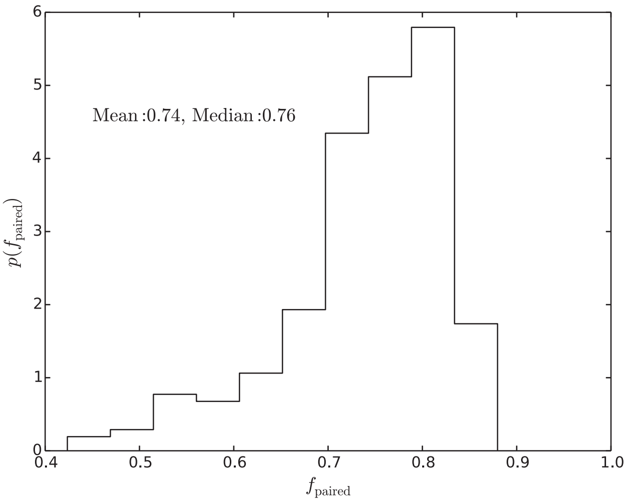

Figure 2. Probability distribution function of $f_{\rm paired}$ for our full halo sample.

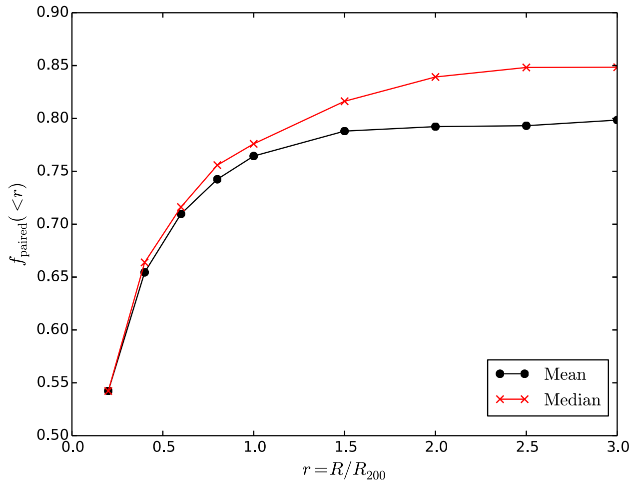

Figure 3. Cumulative paired fraction profiles for the mean (black) and the median (red) values of $f_{\rm paired}(<r)$ for the 100 most massive haloes in our simulation.

also show significant gas–dark matter segregation, with different strength. Intriguingly, the baryonic mass fraction of each halo, $f_b \equiv M_{\rm gas}/(M_{\rm dm} + M_{\rm gas})$, as labelled in each panel, is very close to the universal value, $f_{b,\rm uni} \equiv \Omega_b/\Omega_m = 0.13$ (see also Crain et al. 2007).

It is reasonable to quantify the gas–dark matter segregation strength of a halo using a proxy: the particle paired fraction, $f_{\rm paired}$ is defined as follows. As described in Section 2, the simulated gas and dark matter particles are initially split from an 'original' particle. We define a dark matter and a gas particle split from the same 'original' particle as a *pair*. For each halo at the present day, we count dark matter–gas pairs, $N_{\rm pairs}$, and define a paired fraction

$$f_{\rm paired} \equiv \frac{2N_{\rm pairs}}{N_{\rm tot}}, \tag{5}$$

where $N_{\rm tot}$ is the total number of particles in a halo. With such a definition, $f_{\rm paired} = 0$ means all gas and dark matter particles come from different Lagrangian space and so are completely segregated, and vice versa for $f_{\rm paired} = 1$. The paired fraction values of our four selected haloes are labelled in Fig. 1. Among them, the first one has the highest value, 0.84, meaning that 84 per cent of its particles (dark matter and gas) come from the same Lagrangian space, while it is only half for the third halo.

The probability distribution function (hereafter PDF) of $f_{\rm paired}$ for our whole halo sample is shown in Fig. 2. As can be seen, $f_{\rm paired}$ has a fairly broad distribution with a peak value around $f_{\rm paired} \sim 0.8$. The mean and median values of $f_{\rm paired}$ for the whole halo sample are 0.74 and 0.76, respectively, meaning that, on average 26 per cent of the particles in a halo are initially segregated. The maximum of $f_{\rm paired}$ in our halo sample is 0.88, whereas the minimum is as low as 0.42.

It is interesting to investigate how $f_{\rm paired}$ varies with the distance from the halo centre R. Here, the halo centre is defined as the position of the density maximum of the halo. In Fig. 3, we plot the cumulative profile of $f_{\rm paired}$ for particles within different radii from the halo centre for a stacked halo sample. To ensure that there are enough particles to resolve the inner halo, we only use the 100 most massive haloes with $M_{200} > 3.2 \times 10^{10}\, h^{-1}$ M$_\odot$, which have $\gtrsim$2000 particles for both dark matter and gas inside $R = 0.2R_{200}$, to compute the profile. Note that the distance has been scaled by the virial radius, R_{200}. Clearly the inner particles tend to be more segregated; on average, half of the particles inside $R = 0.2R_{200}$ lost their *partners* in the initial conditions. Interestingly, even at very large radii, $R = 3R_{200}$, the unpaired fraction, $1 - f_{\rm paired}$, is still as large as ~20 per cent.

In order to examine whether $f_{\rm paired}$ depends on halo mass, we plot $f_{\rm paired}$ as a function of halo mass, M_{200}, in Fig. 4 for our halo sample. There is a weak mass dependence of the paired fraction with quite large scatter. On average, galactic haloes have a mean value of $f_{\rm paired} \sim 0.8$, while it is $f_{\rm paired} \sim 0.7$ for dwarf-sized haloes. Note that this weak mass dependence is not a result of numerical resolution effects, as demonstrated in the appendix. Presumably, this mass dependence could be due to the fact that more massive haloes have deeper potential wells and thus are less affected by the surrounding environment.

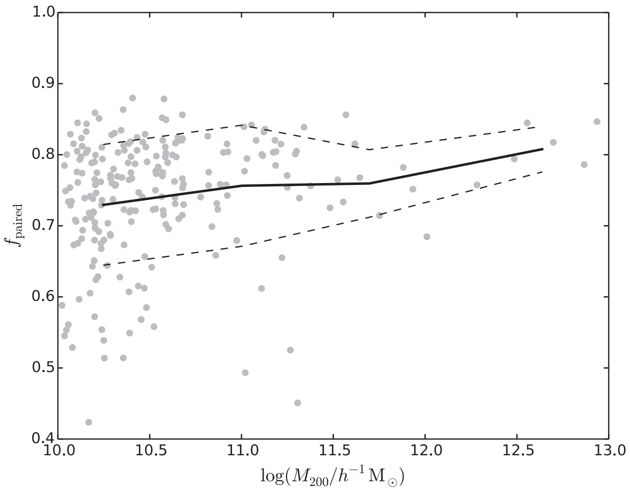

Figure 4. Mass dependence of $f_{\rm paired}$. The thick solid line (thin dashed lines) shows the mean values (standard deviations) of $f_{\rm paired}$ in different mass bins. Each grey dot represents a halo.

4 WHAT CAUSES THE GAS–DARK MATTER SEGREGATION?

What causes the segregation between gas and dark matter during halo assembly? We take a closer look at the assembly history of several representative haloes. Our finding is that complex interplay between dark matter and gas during non-linear interactions account for it, while the resulting physical processes vary from case to case. We list a few major processes below.

In some cases, the segregation is caused by mergers. During the collision of two merging haloes, the collisional gas particles of one halo may merge with the other but the collisionless dark matter counterparts may just pass through and become isolated. The halo may re-accrete gas from its surroundings. In this case, the halo gas and dark matter are completely segregated in the initial conditions. As an example, we present a detailed case for a representative halo, no. 17, which has a mass of $M_{200} = 2.2 \times 10^{11}\ h^{-1}\,{\rm M}_{\odot}$, a radius of $R_{200} = 146\ h^{-1}$ kpc, a total particle number of $N_{\rm tot} = 84307$ and a paired fraction of $f_{\rm paired} = 0.84$. Fig. 5 illustrates how the gas and dark matter components from the same Lagrangian region get eventually segregated. Panel (a) shows the temporal evolution of dark matter particles (blue dots) located within R_{200} of the final $z = 0$ halo, as well as their associated gas partners that are not necessary inside R_{200} at $z = 0$ (red dots). One can easily see that both components are initially perfectly mixed, but they start to segregate a little at $z = 3$, and eventually become more and more segregated during the course of halo clustering. Circles in each plot indicate R_{200} of the final halo. It is quite striking to see that how extended is the distribution of gas partners. Panel (b) shows the temporal evolution of gas particles of the final halo and their dark matter partners. In panel (c), we provide 'zoom-in' images of a patch of panels (a4–6), to illustrate the case of two haloes merging. In this case, the gas component of two haloes mixed, but the dark matter counterpart just passed through.

The segregation can be also caused by 'pancake stripping' as pointed out by Benítez-Llambay et al. (2013) and are also observed in our own simulation. In this case, when a halo passes through a large-scale pancake, its gas component may be entirely stripped by ram-pressure, and leave behind a nearly gas-free halo. An additional case occurs for haloes located in filaments: their gas and dark matter components initially move along a filament together, but during the later evolution, the gas gradually lags behind its dark matter counterpart as it experiences additional pressure forces. In this case, the dark matter and gas are also disjointed in the initial conditions. Other complicated cases also exist, but we do not intend to list all of them here. In short, from what we investigated, the gas–dark matter segregation is a natural outcome of different physics obeyed by gas and dark matter during the non-linear evolution.

The gas–dark matter segregation effect discussed above may question the precision of approaches that use dark matter merger trees to estimate the evolution of gas residing in dark matter haloes, for instance, the standard disc formation and semi-analytical galaxy formation models. As an example, we use this segregation effect to explain the angular momentum misalignment between gas and dark matter component of dark matter haloes below.

5 MISALIGNMENT OF ANGULAR MOMENTUM VECTORS BETWEEN DARK MATTER AND GAS

As we discussed in previous sections, in the standard galaxy formation theory, the dark matter and gas components of a halo are assumed to be perfectly mixed in the initial conditions, and consequently they are assumed to experience exactly the same tidal torques from surrounding density fields and so share the same specific angular momentum. However, as demonstrated in the last section, the gas and dark matter of a halo are segregated in the initial conditions. To examine to what extent the segregation effect predicts a misalignment of the angular momentum vectors between the two components in the initial conditions, in Fig. 6, we plot the PDF of the misalignment angle, θ, for the protohaloes of our sample at $z = 127$ as a red solid line. Here, θ is computed as

$$\theta(z) = \arccos \frac{\boldsymbol{J}_{\rm dm}(z) \cdot \boldsymbol{J}_{\rm gas}(z)}{|\boldsymbol{J}_{\rm dm}(z)||\boldsymbol{J}_{\rm gas}(z)|}, \tag{6}$$

where the angular momentum of the dark matter/gas component at redshift z is

$$\boldsymbol{J}_{\rm dm,gas}(z) = m_{\rm dm,gas} \sum_{i=1}^{N_{\rm dm,gas}} [\boldsymbol{r}_i(z) - \boldsymbol{r}_{\rm cm}(z)] \times [\boldsymbol{v}_i(z) - \boldsymbol{v}_{\rm cm}(z)]. \tag{7}$$

Here, $\boldsymbol{r}_{\rm cm}(z)$ and $\boldsymbol{v}_{\rm cm}(z)$ are the redshift-dependent centre-of-mass position and velocity of the particles that are found in a halo at $z = 0$, respectively.

The misalignment angles θ of protohaloes have a broad distribution with a mean (median) value of $31\overset{\circ}{.}4$ ($20\overset{\circ}{.}2$), which is contrary to expectation from the well-mixed assumption of gas and dark matter in the initial conditions. For ease of comparison, we also plot the PDF of θ for the $z = 0$ counterparts as a black solid line. It is quite striking that the distribution of θ for the $z = 0$ haloes is almost identical to their counterparts in unevolved stage in the initial conditions. In other words, the angular momentum misalignment we see today is already present in the initial conditions. Note that the PDF of θ for our $z = 0$ haloes is in good agreement with previous studies (see e.g. van den Bosch et al. 2002; Sharma & Steinmetz 2005).

In Fig. 7, we plot the misalignment angle of each halo in our sample at $z = 0$ against its protohalo counterpart in the initial conditions. Clearly, the misalignment angles at these two epochs exhibit a strong correlation, with a Spearman's rank coefficient $r = 0.518$ and p-value of 5.4×10^{-17}. Note, in order to show the correlation for the data points with small angles more clearly, we plot

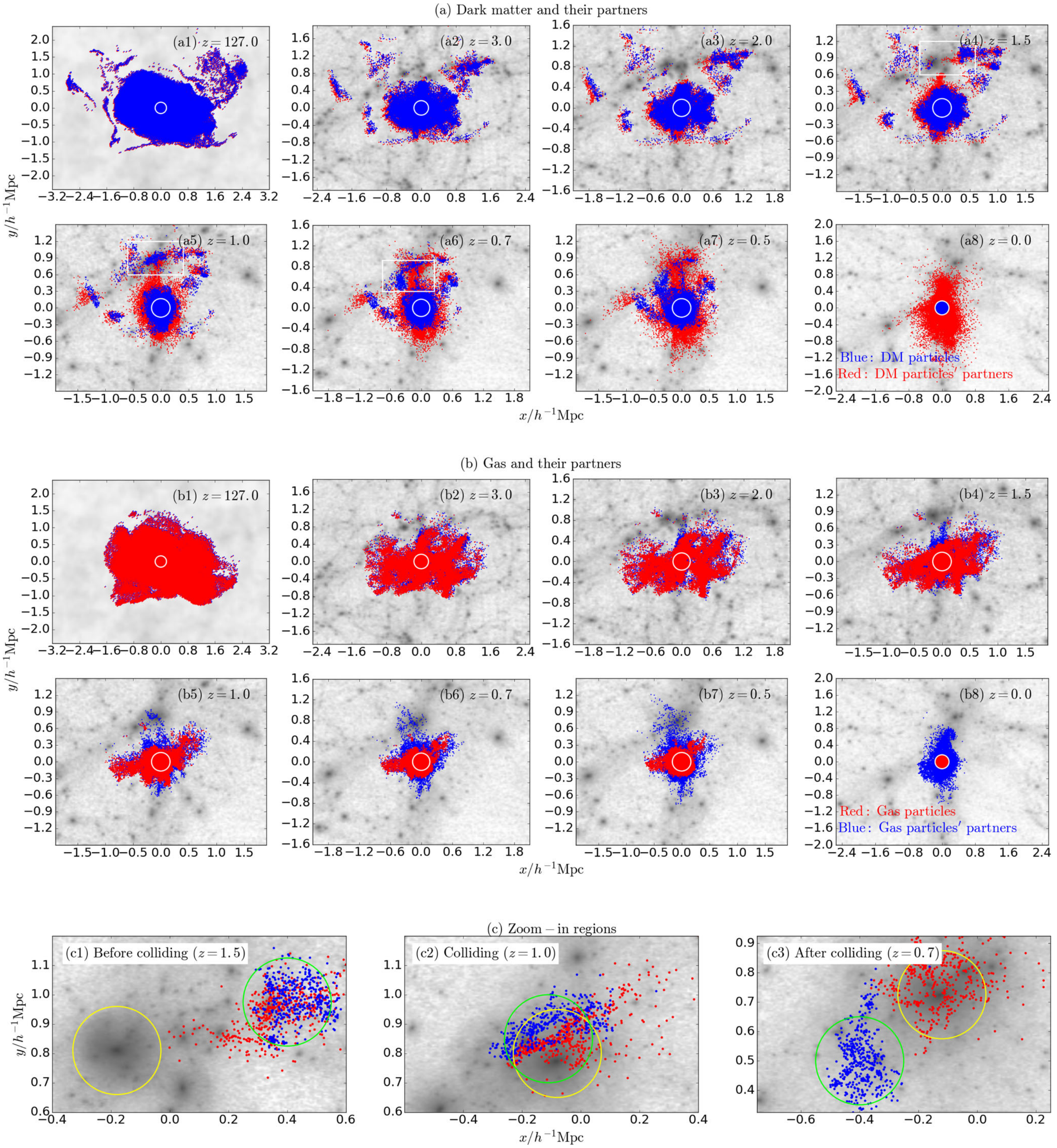

Figure 5. (a) Time evolution of dark matter particles (blue dots) of halo no. 17 and their associated gas partners (red dots). The white circles represent R_{200} of the final halo. The white rectangles in panels (a4–6) mark the 'zoom-in' regions that are further shown in panels (c1–3). (b) Similar to panel (a), but for the gas particles (red dots) of the same halo and their dark matter partners (blue dots). (c) 'Zoom-in' images of the patches marked in panels (a4–6) to illustrate the collision of two merging haloes (green and yellow circles). Note, to illustrate the segregation effect clearly, in panel (c), we only plot those dark matter particles (blue dots) in the halo marked with a green circle and their gas partners (red dots).

log θ here. But the Spearman's rank coefficient and p-value shown in the upper-left corner are calculated directly from θ. Such a strong correlation may be understood as follows. According to the tidal torque theory, a halo's angular momentum is mainly accumulated during the linear evolution and does not evolve much after collapse because collapsed objects dramatically reduce their spatial extent and separate from each other (see e.g. Peebles 1969; Sugerman, Summers & Kamionwski 2000; Porciani, Dekel & Hoffman 2002). We thus expect that, once established in the linear regime, the mean/median misalignment angle of our halo sample will not vary significantly during the later non-linear evolution. This is illustrated in Fig. 8, where we present the time evolution of the misalignment

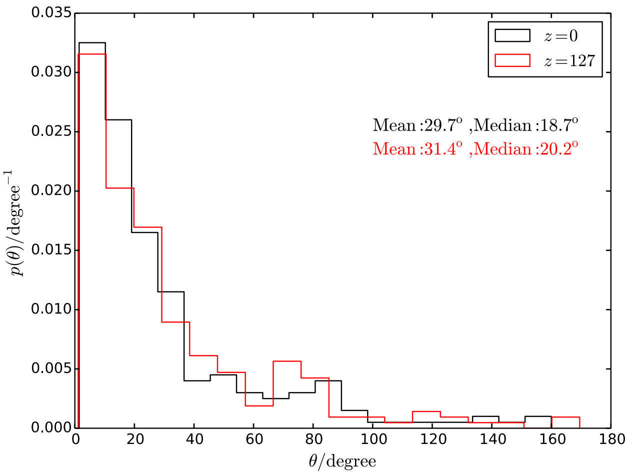

Figure 6. Probability distribution function of the misalignment angle, θ, for present-day haloes (black) and their protohalo counterparts at $z = 127$ (red).

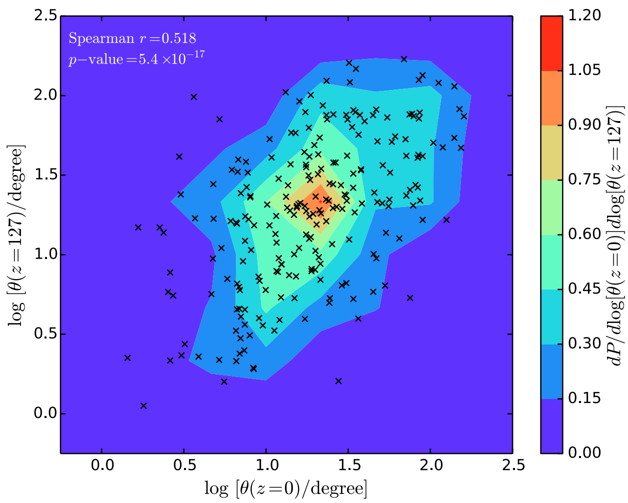

Figure 7. Correlation between $\theta(z = 127)$ and $\theta(z = 0)$ for our halo sample. The contours show the 2D probability distribution function calculated from the data points that are marked as crosses.

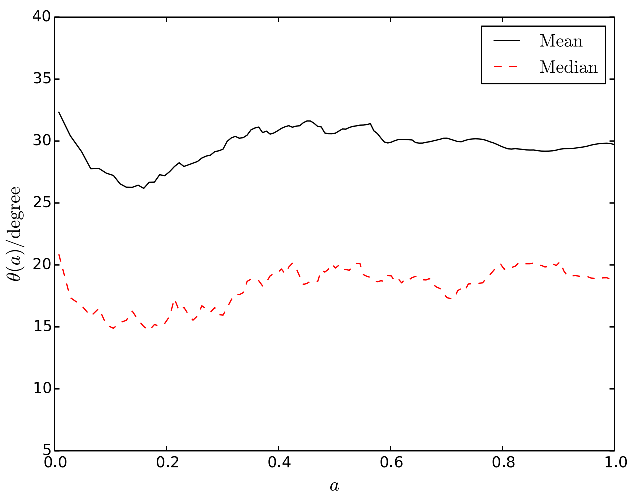

Figure 8. Time evolution of θ of protohaloes. The mean and median of θ are shown as solid and dashed lines, respectively.

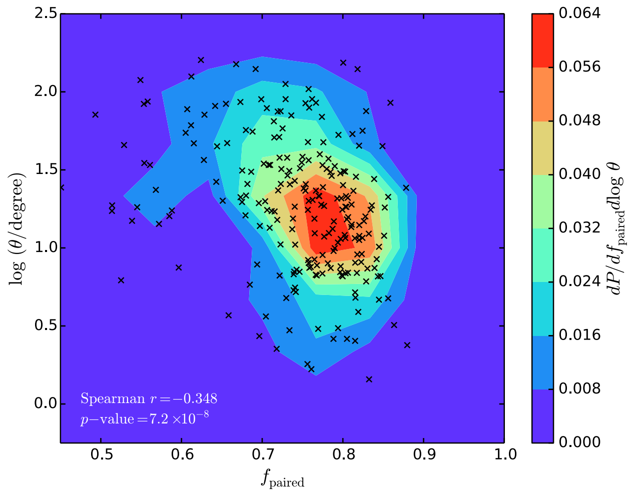

Figure 9. Similar to Fig. 7, but for the correlation between θ and $f_{\rm paired}$.

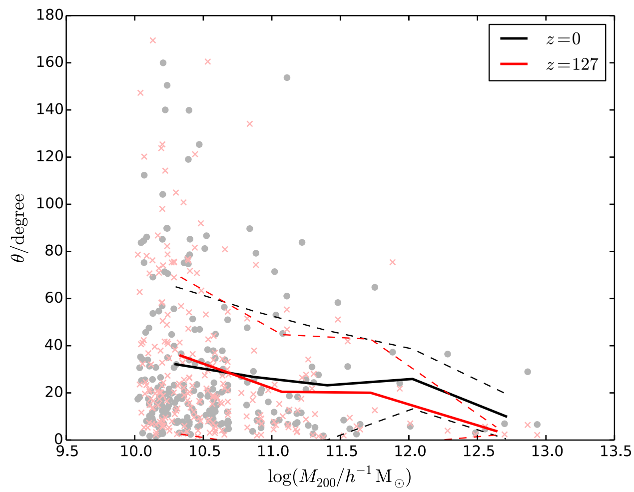

Figure 10. Similar to Fig. 4, but for the mass dependence of the misalignment angle, θ, in the initial conditions (red) and at $z = 0$ (black).

angle between gas and dark matter of the 100 most massive haloes in our simulation; the mean and median values of the misalignment angles are shown at each recorded snapshot. Clearly, the mean value of the misalignment angle only fluctuates mildly with an amplitude smaller than $\sim 5^\circ$ during the whole evolution, consistently with our expectation.

To further investigate explicitly the relationship between the misalignment and the segregation strength, in Fig. 9, we plot the correlation between the misalignment angle, θ, and the segregation strength proxy, $f_{\rm paired}$. As shown in the plot, a halo that has a stronger segregation tends to have a larger misalignment angle. This correlation is quite strong with a Spearman's rank coefficient $r = -0.348$ and p-value of 7.2×10^{-8}.

As demonstrated in Fig. 4, the segregation strength proxy, $f_{\rm paired}$, depends weakly on halo mass. It is natural to expect that the misalignment angle should also depend on halo mass. Since the paired fraction correlates with halo mass, and the spin misalignment anticorrelates with the paired fraction, we expect an anticorrelation between the misalignment angle and halo mass. This expectation is confirmed by Fig. 10, in which we plot θ versus M_{200} for our halo sample, with the mean value shown as a black solid line. Note that this result is consistent with previous studies (see e.g. van den Bosch et al. 2002).

In summary, the above results suggest that the dark matter and gas components of a present-day halo are segregated in the initial conditions and so have different angular momentum vectors. This difference is preserved during later halo assembly and can be understood with the tidal torque theory. This naturally explains the angular momentum misalignment of dark matter haloes observed at $z = 0$. This explanation is different from that of Sharma et al. (2012) who suggested that the misalignment comes from galaxy mergers when the intrinsic spins of progenitors are not aligned with the orbital angular momentum. It also differs from the explanation of Prieto et al. (2015) who argued that additional pressure torques in the gas lead to the misalignment. Our results, which are based on a large halo sample from a cosmological simulation, naturally and self-consistently explain various observed facts in numerical simulations and thus offer a simple and clear explanation to the puzzling misalignment problem.

6 CONCLUSION

In the current galaxy formation theory, the dark matter and gas components of a halo are assumed to be well mixed in the initial conditions before they are segregated due to radiative cooling. In this study, we have used non-radiative *N*-body/SPH hydrodynamical simulations to examine this assumption and investigate the segregation of gas and dark matter during halo assembly.

By tracing particles of present-day haloes to the initial conditions, we find that the dark matter and gas components of haloes are often initially segregated to varying degrees. When using the paired fraction as a proxy to measure the segregation strength of haloes, we find that on average ∼25 per cent of the particles (dark and baryonic) in a halo originates from different Lagrangian regions. The segregation strength varies with halo mass, with more massive haloes tending to be less segregated. The paired fraction is about 80 per cent for haloes with mass larger than $10^{12.5}\,h^{-1}\,\mathrm{M}_{\odot}$ and decreases to 70 per cent for haloes with mass about $10^{10}\,h^{-1}\,\mathrm{M}_{\odot}$. The segregation strength of a halo is stronger in the inner halo and persists to very outer parts, $\sim 3 \times R_{200}$. Dark matter and gas follow different underlying physics and this leads to segregation during hierarchical halo assembly.

The gas–dark matter segregation has important implications for galaxy formation theory. As an example, the segregation explains the misalignment between the angular momentum vectors of gas and dark matter seen in previous hydrodynamical simulations of galaxy formation. As the dark matter and gas components of a present-day halo are segregated in the initial conditions, they experience different tidal torques and therefore end up with different angular momentum vectors. This difference is preserved during later halo assembly. Consequently the PDF of $z = 0$ haloes and their counterparts in the initial conditions are almost identical. For individual haloes, there is a tight correlation between the misalignment angles at $z = 0$ and of its protohalo in the initial conditions, and the segregation strength proxy, f_{paired}, correlates with the misalignment angle quite strongly. All these facts support our argument about the origin of the misalignment between the angular momentum vectors of dark matter and gas in haloes.

The results presented in this paper challenge the precision of semi-analytical approaches based on the use of dark matter merger trees to estimate the evolution of gas resident in dark matter haloes.

ACKNOWLEDGEMENTS

We thank simulating discussions with Prof. Simon White. LG acknowledges support from the NSFC grant (nos. 11133003, 11425312) and a Newton Advanced Fellowship, as well as the hospitality of the Institute for Computational Cosmology at Durham University. CSF acknowledges ERC Advanced Grant COSMIWAY. QG acknowledges support from the NSFC grant (nos. 11573033, 11622325), the 'Recruitment Program of Global Youth Experts' of China, the NAOC grant (Y434011V01) and a Newton Advanced Fellowship. JW acknowledges the 973 programme grant 2015CB857005 and NSFC grant no. 11373029, 11390372.

REFERENCES

Baugh C. M., 2006, Rep. Prog. Phys., 69, 3101
Benítez-Llambay A. et al., 2013, ApJ, 763, L41
Benson A. J., 2010, Phys. Rep., 495, 33
Bett P., Eke V., Frenk C. S., Jenkins A., Okamoto T., 2010, MNRAS, 404, 1137
Catelan P., Theuns T., 1996, MNRAS, 282, 455
Chen D. N., Jing Y. P., Yoshikaw K., 2003, ApJ, 597, 35
Crain R. A. et al., 2007, MNRAS, 377, 41
Croft R. A. C., Di Matteo T., Springel V., Hernquist L., 2009, MNRAS, 400, 43
Doroshkevich A. G., 1970, Astrofizika, 6, 581
Eisenstein D. J., Hu W., 1998, ApJ, 496, 605
Fall S. M., Efstathiou G., 1980, MNRAS, 193, 189
Frenk C. S., White S. D. M., 2012, Ann. Phys., 524, 507
Guo Q. et al., 2011, MNRAS, 413, 101
Hahn O., Teyssier R., Carollo C. M., 2010, MNRAS, 405, 274
Hoyle F., 1951, in Burgers J. M., van de Hulst H. C., eds, Problems of Cosmical Aerodynamics. Central Air Documents Office, Dayton, p. 195
Kauffmann G., Colberg J. M., Diaferio A., White S. D. M., 1999, MNRAS, 303, 188
Knebe A. et al., 2015, MNRAS, 451, 4029
Knollmann S. R., Knebe A., 2009, ApJS, 182, 608
Lynden-Bell D., 1967, MNRAS, 136, 101
Mo H. J., Mao S., White S. D. M., 1998, MNRAS, 295, 319
Peebles P. J. E., 1969, ApJ, 155, 393
Porciani C., Dekel A., Hoffman Y., 2002, MNRAS, 332, 325
Prieto J., Jimenez R., Haiman Z., González R. E., 2015, MNRAS, 452, 784
Sharma S., Steinmetz M., 2005, ApJ, 628, 21
Sharma S., Steinmetz M., Bland-Hawthorn J., 2012, ApJ, 750, 107
Somerville R. S., Davé R., 2015, ARA&A, 53, 51
Springel V., 2005, MNRAS, 364, 1105
Springel V., White S. D. M., Tormen G., Kauffmann G., 2001, MNRAS, 328, 726
Sugerman B., Summers F. J., Kamionwski M., 2000, MNRAS, 311, 762
van den Bosch F. C., Abel T., Croft R. A. C., Hernquist L., White S. D. M., 2002, ApJ, 576, 21
van den Bosch F. C., Abel T., Hernquist L., 2003, MNRAS, 346, 177
White S. D. M., 1984, ApJ, 286, 34
White S. D. M., 1996, in Schaefer R., Silk J., Spiro M., Zinn-Justin J., eds, Cosmology and Large-Scale Structure. Elsevier, Amsterdam, p. 349
White S. D. M., Frenk C. S., 1991, ApJ, 379, 52
White S. D. M., Rees M. J., 1978, MNRAS, 183, 341
Yoshida N., Abel T., Hernquist L., Sugiyama N., 2003, ApJ, 592, 645
Zel'dovich Ya. B., 1970, A&A, 5, 84
Zjupa J., Springel V., 2017, MNRAS, 466, 1625

APPENDIX: NUMERICAL CONVERGENCE TESTS

We have performed two additional simulations with $128^3 \times 2$ and $512^3 \times 2$ particles, respectively. Their initial conditions have the

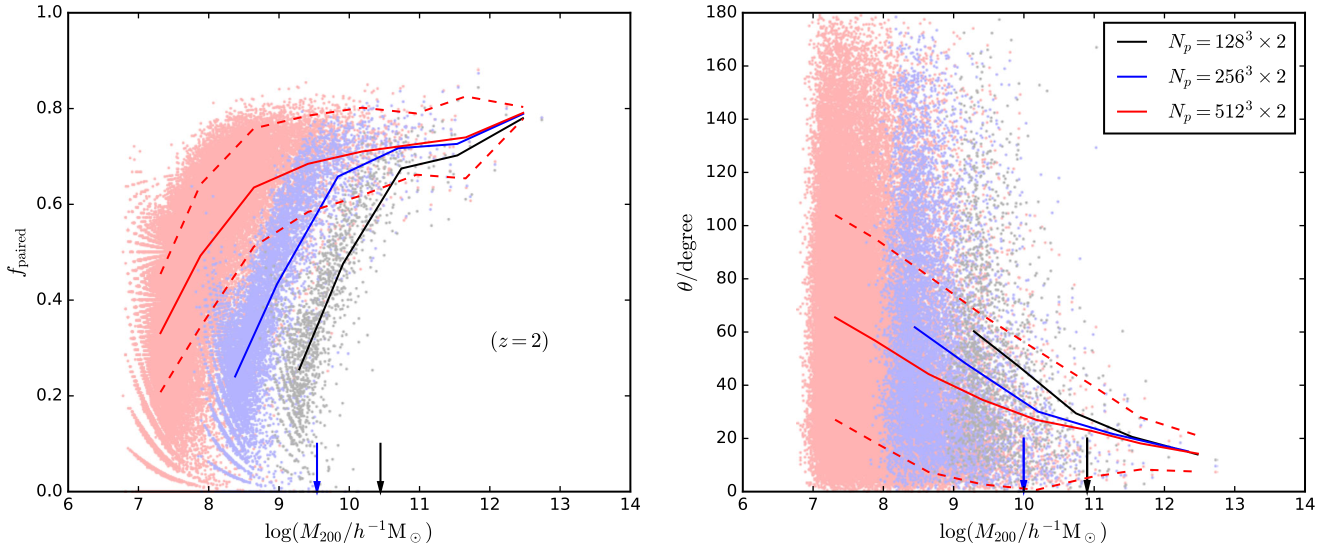

Figure A1. Resolution convergence for haloes' paired fractions (left) and misalignment angles (right) at $z = 2$. The scatters plot all haloes with $\geq$10 dark matter particles and $\geq$10 gas particles from the $128^3 \times 2$ (black), $256^3 \times 2$ (blue) and $512^3 \times 2$ (red) simulations. The solid lines represent the mean values at different mass bins. To be clear, we only plot the standard deviation for the $512^3 \times 2$ simulation (dashed lines). The black and blue arrows mark the masses of convergence at a 15 per cent level for the $128^3 \times 2$ and $256^3 \times 2$ simulations, respectively.

same random phases as the fiducial $256^3 \times 2$ simulation presented in the main text. These simulations have been carried out to $z = 2$. All haloes with at least 10 dark matter particles and 10 gas particles are identified in these simulations.

In the left-hand panel of Fig. A1, we plot the paired fraction, $f_{\rm paired}$, against the virial mass, M_{200}, of each halo for the three simulations; different colours distinguish different simulations, as labelled in the legend. The solid lines display the respective median values in each mass bin. There is a good convergence between the results from the $512^3 \times 2$ and $256^3 \times 2$ for haloes more massive than $M_{200} \geq 3.5 \times 10^9\ h^{-1}\,{\rm M}_\odot$, and from the $256^3 \times 2$ and $128^3 \times 2$ for haloes more massive than $M_{200} \geq 2.8 \times 10^{10}\ h^{-1}\,{\rm M}_\odot$. For both mass scales, haloes with $\gtrsim$700 dark matter particles and $\gtrsim$700 gas particles in the lower resolution simulation tend to agree with the higher resolution runs with a difference of less than ∼15 per cent. The right-hand panel presents convergence test for the misalignment angles. For haloes with at least 2000 dark matter and gas particles, their misalignment angle measurements are free from resolution effects. Hence, in this study, we only include dark matter haloes with least 2000 for both dark matter and gas particles in our halo sample.

This paper has been typeset from a TEX/LATEX file prepared by the author.